Equatorial Kelvin wave signatures in ozone column measurements from the Global Ozone Monitoring Experiment (GOME)

R. M. A. Timmermans, R. F. van Oss, and H. M. Kelder[1]
Royal Netherlands Meteorological Institute, De Bilt, Netherlands

Received 3 July 2003; revised 18 September 2003; accepted 27 October 2003; published 3 January 2004.

[1] This study investigates tropical Kelvin wave signatures in the total ozone column data from the Global Ozone Monitoring Experiment (GOME) instrument. A new approach for spectral analysis is introduced by generalizing an unequally spaced data technique from one to two dimensions. This enables the handling of satellite data containing gaps. The simple statistical behavior of the method furthermore allows an easy determinination of the statistical significance of any observed spectral features. Seven years of GOME data (1995–2002) have been analyzed in which we have identified three periods of high Kelvin wave activity in 1996, 1998, and 2000. The periods are in conjunction with westward equatorial zonal winds at 30 hPa and show eastward propagating waves 1–2 with periods of ~12–15 days. The induced Kelvin wave signatures in the ozone concentrations are around 2–4 DU peak-to-peak and can be attributed to "slow" Kelvin waves. The results are shown to be significant. Our study provides an important contribution to the study of Kelvin waves by introducing the bidimensional unequally spaced data spectral analysis and is the first to demonstrate the potential of the GOME ozone data set to contribute to a global description of equatorial Kelvin wave activity. *INDEX TERMS:* 3334 Meteorology and Atmospheric Dynamics: Middle atmosphere dynamics (0341, 0342); 3384 Meteorology and Atmospheric Dynamics: Waves and tides; 3360 Meteorology and Atmospheric Dynamics: Remote sensing; 3374 Meteorology and Atmospheric Dynamics: Tropical meteorology; *KEYWORDS:* GOME, Kelvin, waves

Citation: Timmermans, R. M. A., R. F. van Oss, and H. M. Kelder (2004), Equatorial Kelvin wave signatures in ozone column measurements from the Global Ozone Monitoring Experiment (GOME), *J. Geophys. Res.*, *109*, D01101, doi:10.1029/2003JD003946.

1. Introduction

[2] Planetary scale equatorial waves play an important role in the dynamics of the tropical atmosphere. Forced by large-scale unsteady convective heating and accompanying latent heat release, these waves propagate horizontally and vertically carrying momentum into the middle and upper atmosphere.

[3] The Kelvin wave is one of the most dominant equatorial waves. The change in sign of the Coriolis parameter at the equator allows this special type of equatorial wave to exist. It is an eastward propagating wave characterized by zonal velocity and geopotential perturbations varying in latitude as Gaussian functions centered at the equator. The waves also induce temperature fluctuations because of adiabatic heating and cooling when air parcels are vertically displaced.

[4] The observed Kelvin waves are primarily of zonal wave number 1 or 2 and have periods in the lower stratosphere of about 15 days [*Holton*, 1992]. Furthermore, Kelvin waves are mainly detected when the mean flow is westward because waves are absorbed or reflected when their phase velocity is in the same direction as the background current and only waves that head against the current can penetrate it. Thus, in case of a mean westward flow, the eastward heading Kelvin waves can propagate into the middle and upper stratosphere. There they are absorbed, and the eastward momentum carried upward by the Kelvin waves is transferred to the background flow. The transfer of momentum causes an eastward acceleration of the current and eventually a reverse from westward to eastward. The reversal in the winds begins in upper levels and propagates downward in time. The same process takes place for the westward traveling Rossby-gravity waves but in the opposite direction. The Rossby-gravity waves penetrate the eastward mean zonal flow carrying westward momentum upward into the upper stratosphere where the momentum is transferred to the background current. The momentum provided by the Kelvin and Rossby-gravity waves together with gravity waves is believed to be responsible for driving the quasi-biennial oscillation (QBO) of the zonal mean winds in the lower stratosphere and the semiannual oscillation (SAO) in the upper stratosphere and mesosphere [*Canziani and Holton*, 1998, and references herein]. Both these oscillations are important features in the global circulation.

[5] In addition to temperature fluctuations, Kelvin waves also induce fluctuations in the ozone concentrations. In the upper stratosphere where ozone has a short chemical life-

[1] Also at Eindhoven University of Technology, Eindhoven, Netherlands.

0148-0227/04/2003JD003946$09.00

time and a temperature-dependent equilibrium concentration, this takes place through the temperature dependence of the photochemical reactions. In the lower atmosphere where ozone has a strong vertical gradient and a long photochemical lifetime this takes place through motions. Thus both temperature as well as ozone observations can be used to identify Kelvin waves.

[6] One of the earliest observational studies on Kelvin waves was done by *Wallace and Kousky* [1968]. Using wind and temperature measurements from radiosondes they identified "slow" Kelvin waves in the lower stratosphere with periods of about 2 weeks. *Hirota* [1978] made use of rocketsonde temperature and wind observations to show evidence of the "fast" Kelvin waves in the upper stratosphere and mesosphere with periods of about 7 days.

[7] With the availability of satellite observations, the global structure of the Kelvin waves has been investigated. Fast Kelvin waves were identified in the temperature and ozone measurements from the Limb Infrared Monitor of the Stratosphere (LIMS) and Solar Backscatter Ultraviolet (SBUV) instruments on board the Nimbus-7 spacecraft [*Salby et al.*, 1984, 1990; *Randel*, 1990; *Randel and Gille*, 1991] and the Improved Stratospheric And Mesospheric Sounder (ISAMS) [*Stone et al.*, 1995] and Microwave Limb Sounder (MLS) [*Canziani et al.*, 1994, 1995] on board the Upper Atmosphere Research Satellite (UARS).

[8] Slow Kelvin waves in the lower stratosphere need observations with a sufficiently high vertical resolution to get resolved. They have been observed in temperature and ozone profiles retrieved from measurements by LIMS [*Kawamoto et al.*, 1997] and Cryogenic Limb Array Etalon Spectrometer (CLAES) [*Shiotani et al.*, 1997; *Canziani and Holton*, 1998], the latter on board UARS. The limited time periods covered by the LIMS and CLAES measurements do however not allow the study of the variability of slow Kelvin waves over more than two years and by that the conjunction with the QBO cycle.

[9] Total ozone column measurements also appear to be sensitive to slow Kelvin waves in the lower stratosphere.

[10] *Ziemke and Stanford* [1994] found tropical Kelvin wave signatures in the Nimbus-7 TOMS (Total Ozone Mapping Spectrometer) total column ozone data covering November 1978 to January 1992. Observed periods for zonal waves 1–2 were ~5–15 days with amplitudes of the induced ozone perturbations around 3 DU. This is in agreement with model calculations presented in the same study suggesting that Kelvin waves should dynamically induce total ozone perturbations of a few DU.

[11] Reproducing a realistic QBO and Kelvin waves in atmospheric models has been proven to be difficult [*Pawson*, 1992; *Takahashi*, 1996, 1999; *Hamilton et al.*, 1999]. However, many improvements are being made. *Amodei et al.* [2001] compared tropical oscillations and planetary scale Kelvin waves in four troposphere-stratosphere climate models and the assimilated data set produced by the UK Met Office (UKMO). None of the four models reproduced a wind structure that resembles the QBO. Despite this, all four models are able to generate Kelvin waves with amplitudes close to those observed in the MLS and CLAES data in the lower stratosphere. In three of the models the absence of a QBO allows Kelvin waves to propagate up into the upper stratosphere and mesosphere, where their amplitude grows. Consequently, the Kelvin wave amplitudes in these three models are overestimated in the upper stratosphere and mesosphere.

[12] This present study shows that the GOME ozone column data exhibit features that can be attributed to tropical Kelvin waves. Three periods have been identified with high Kelvin wave activity. The significance of the results has been verified by statistical analysis.

[13] In spite of their importance in the atmosphere, a climatology of tropical Kelvin waves does not exist. This study demonstrates the potential of the GOME measurements to contribute to the derivation of such a climatology.

2. GOME Measurements

[14] The Global Ozone Monitoring Experiment (GOME) instrument flies on board of the second European Remote Sensing Satellite (ERS-2), which was launched on 21 April 1995. GOME is a nadir viewing spectrometer that measures the direct solar irradiance and the solar radiation scattered by Earth's atmosphere and surface in the ultraviolet and visible wavelength range of 240 to 790 nm at a spectral resolution of 0.2–0.4 nm. GOME scans the Earth surface with a spatial resolution of 40 km in latitudinal and 320 km in longitudinal direction. Global coverage is reached within 3 days. Total ozone column values are retrieved from the ratio of the radiance and irradiance spectra by utilizing the characteristic spectral absorption of ozone in part of the Huggins band (325–335 nm). The technique used for the retrieval is based on the DOAS (Differential Optical Absorption Spectroscopy) method [*Platt*, 1994; *Burrows et al.*, 1998]. The amount of ozone below the cloud top, which is called the ghost vertical column, can not be detected by GOME and is therefore derived from a climatological ozone profile. For this study we have used GOME GDP (GOME Data Processing) version 2.7 total ozone column data [*Spurr et al.*, 2002].

[15] The accuracy of the retrieved ozone columns in the tropics is of particular importance for this study. The relative error (precision) of the GDP 2.7 total ozone is of the order of 1% (shown by data assimilation; *Eskes et al.* [2003]). Comparison of GOME total ozone columns with Brewer and Dobson measurements shows differences smaller than 3% in the tropics [*Balis et al.*, 2001]. The agreement between the GOME and TOMS total ozone measurements is generally good [*Bramstedt et al.*, 2002; *Lambert et al.*, 2000]. However, at the equatorial latitudes TOMS values are ~3–5% higher than both GOME and TOVS ozone columns [*Corlett and Monks*, 2001].

[16] The multispectral DOAS method used in the GOME ozone retrieval has several advantages compared to the TOMS algorithm which is based on wavelength pairs and triplets [*Mc Peters et al.*, 1998; *Martin et al.*, 2002; *Valks et al.*, 2003]. The GOME algorithm is less sensitive to aerosols and deviations from the assumed surface albedo.

3. Analysis Method

[17] The ozone column measurements from GOME are taken at variable latitudes and longitudes. To obtain an ozone time series on a fixed latitude-longitude grid we have defined a set of 5° × 5° grid cells covering the latitude band from 2.5°S to 2.5°N and all longitudes. This latitude band is

chosen because the Kelvin waves reach maximum amplitude at the equator. For each grid cell we collect all cloud-free measurements in a 3 day period with center coordinates within the grid cell and compute the average ozone density.

[18] We have only used the cloud-free ground pixels (cloud fraction < 0.1), since GOME measurements in case of clouds suffer from uncertainties in the ghost vertical column, as described above. About half of the total number of GOME measurements in the tropics are cloud-free, resulting in about 5–40 measurements per grid cell over a period of 3 days. Averaging over these measurements increases the precision of the used values from ~1% to ~0.2–0.5%. A possible bias in the data will be filtered out by the spectral analysis and will thereby not influence the results.

[19] In the past several different spectral techniques have been applied to detect Kelvin wave signals in satellite measurements, most of them based on the Fourier transform, which is applied to switch from a representation of the data as function of time and space to a representation of the data as function of wave number and frequency. To determine which wave numbers and frequencies are dominant in the data, the periodogram can be calculated, which is defined as the spectral power (square of the Fourier amplitude) as function of angular frequency ω and zonal wave number *k*.

[20] In this study we have used a method of spectral analysis developed by Lomb [*Press et al.*, 1992], and further elaborated by *Scargle* [1982]. This method of spectral analysis can be applied to unevenly sampled data, and was first used in the work of *Canziani* [1999]. Satellite data sets often contain gaps both in space and time which are not easily handled. The use of interpolation techniques to fill in the gaps are generally not satisfactory. For example, long gaps in the data can produce misleading power at low frequencies corresponding to wavelengths comparable to the gaps [*Press et al.*, 1992]. The method developed by Lomb (which we will call Lomb periodogram) can be applied to unevenly sampled data without the use of interpolation techniques, it simply evaluates the data at the actually measured locations and times. Another important reason to use this technique is its favorable statistical behavior, explicated below, which permits the evaluation of the reliability of an observed spectral signal.

[21] Consider a variable h measured at times t_j with j = 1, 2, …, N. The classical periodogram in one dimension, based on discrete fourier transformation (DFT), is then defined as:

$$P(\omega) \equiv \frac{1}{N}\left[\left(\sum_{j=1}^{N} h(t_j)\cos\omega t_j\right)^2 + \left(\sum_{j=1}^{N} h(t_j)\sin\omega t_j\right)^2\right]. \quad (1)$$

In case of even sampling (time between consecutive measurements is constant), the statistical distribution of this periodogram is simple and makes it easy to determine the significance of an observed spectral feature. In contrary, when the data are sampled at arbitrary t_j's, the statistical distribution is much more complicated. The Lomb periodogram is a modified version of the classical periodogram that does have a simple statistical behavior even in the case of uneven sampling. Again consider the variable h measured at times t_j with j = 1, 2, …, N. The Lomb normalized periodogram in one dimension is then defined as:

$$P_N(\omega) \equiv \frac{1}{2\sigma^2}\left[\frac{\left[\sum_j (h_j-\bar{h})\cos(\omega(t_j-\tau))\right]^2}{\sum_j \cos^2(\omega(t_j-\tau_1))} + \frac{\left[\sum_j (h_j-\bar{h})\sin(\omega(t_j-\tau))\right]^2}{\sum_j \sin^2(\omega(t_j-\tau))}\right] \quad (2)$$

with

$$\tau = \frac{1}{2\omega}\mathrm{a\,tan}\left[\frac{\sum_j \sin 2\omega t_j}{\sum_j \cos 2\omega t_j}\right] \quad (3)$$

$$\bar{h} \equiv \frac{1}{N}\sum_{j=1}^{N} h(t_j) \quad (4)$$

$$\sigma^2 \equiv \frac{1}{N-1}\sum_{j=1}^{N}(h(t_j)-\bar{h})^2. \quad (5)$$

[22] Because we are dealing with GOME data in two dimensions, i.e., as function of time and longitude, we have extended the Lomb method from one to two dimensions. We consider a two dimensional data set consisting of N_{tot} data points. The functional value is denoted by $h_{j,l} \equiv h(t_j, x_l)$ measured at times t_j with j = 1, 2, …, N_t and locations x_l with l = 1, 2, …, N_x. The Lomb normalized periodogram as function of angular frequency ω and zonal wave number *k* is given by:

$$P_N(\omega,k) \equiv \frac{1}{2\sigma^2}\left[\frac{\left[\sum_{j,l} (h_{j,l}-\bar{h})\cos(\omega(t_j-\tau_1)\pm k(x_l-\tau_2))\right]^2}{\sum_{j,l}\cos^2(\omega(t_j-\tau_1)\pm k(x_l-\tau_2))} + \frac{\left[\sum_{j,l} (h_{j,l}-\bar{h})\sin(\omega(t_j-\tau_1)\pm k(x_l-\tau_2))\right]^2}{\sum_{j,l}\sin^2(\omega(t_j-\tau_1)\pm k(x_l-\tau_2))}\right] \quad (6)$$

with

$$\tau_1 = \frac{1}{2\omega}\mathrm{a\,tan}\left[\frac{\sum_j \sin 2\omega t_j}{\sum_j \cos 2\omega t_j}\right] \quad (7)$$

$$\tau_2 = \frac{1}{2k}\mathrm{a\,tan}\left[\frac{\sum_l \sin 2kx_l}{\sum_l \cos 2kx_l}\right] \quad (8)$$

$$\bar{h} \equiv \frac{1}{N_{tot}}\sum_{j=1}^{N_t}\sum_{l=1}^{Nx} h(x_l,t_j) \quad (9)$$

$$\sigma^2 \equiv \frac{1}{N_{tot}-1}\sum_{j=1}^{N_t}\sum_{l=1}^{Nx}(h(x_l,t_j)-\bar{h})^2. \quad (10)$$

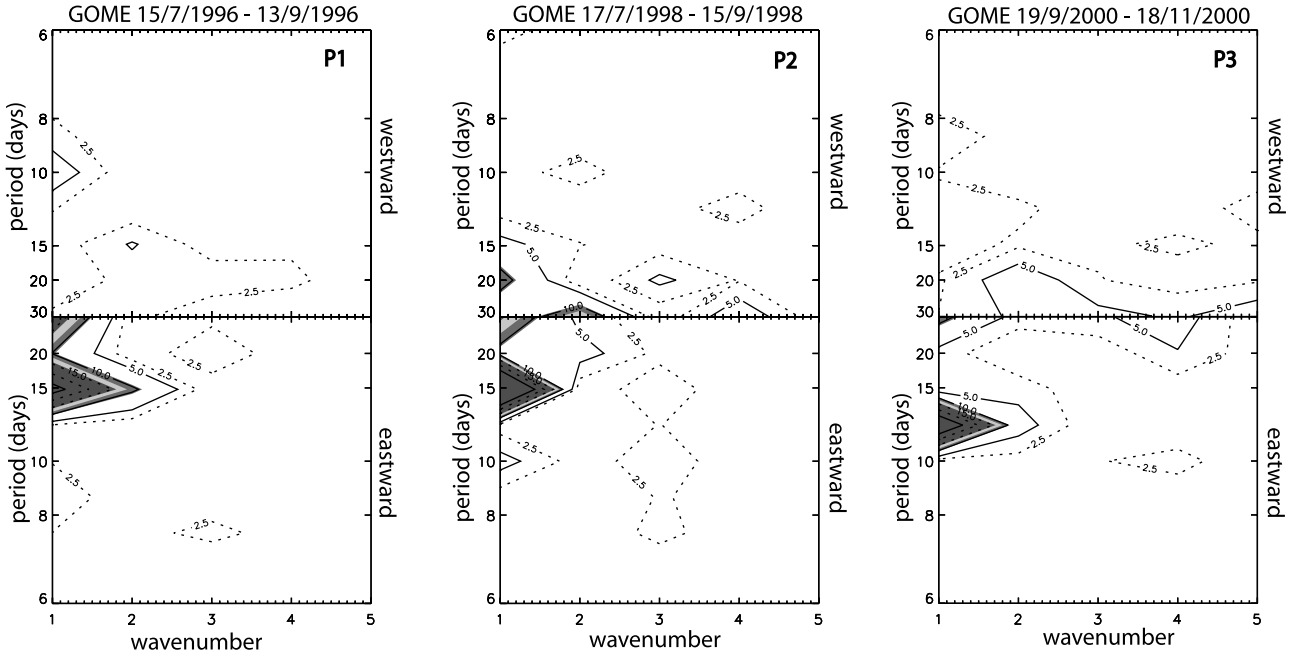

Figure 1. Lomb periodogram for the GOME ozone columns for three different periods. See color version of this figure at back of this issue.

[23] The plus sign in equation (6) corresponds to westward traveling waves and the minus sign to eastward traveling waves.

[24] Because the periodogram of noisy data also is noisy, it can exhibit large spurious peaks that should not be mistaken for a periodic signal. Therefore it is necessary to evaluate the significance of an observed spectral peak in the periodogram. The statistical significance of a spectral peak is found by considering the probability that it could have arisen from noise fluctuations. We have chosen for the Lomb normalized periodogram because this probability is easily determined from the simple statistical behaviour of the Lomb periodogram even in the case of unequally spaced data. In case $h_{j,l}$ would be pure Gaussian noise, P_N at any particular ω and k is exponentially distributed with unit mean. Hence the probability that P_N (ω, k) for arbitrary ω and k will lie between z and $z + dz$ is $\exp(-z)dz$. If we scan M-independent frequencies, the probability that none give values larger than z is $(1 - e^{-z})^M$. So the probability that one frequency gives a peak larger than z is:

$$Pr(>z) \equiv 1 - (1 - e^{-z})^M. \tag{11}$$

[25] A small value of this probability means there is a small chance that the peak is caused by noise and thus indicates a highly significant periodic signal. Equation (11) leads to the following detection threshold [*Scargle*, 1982]:

$$z_0 = -\ln\left[1 - (1 - p_0)^{\frac{1}{M}}\right]. \tag{12}$$

[26] An observed power exceeding this detection threshold z_0 has a p_0 probability of being caused by pure noise. Accordingly, using $p_0 = 0.01$, a power exceeding z_0 indicates a 99% significant periodic signal.

4. Results

[27] Figure 1 shows the periodogram P_N as function of wave number and period for three 60-day time periods (P1: 15 July to 13 September 1996; P2: 17 July to 15 September 1998; P3: 19 September to 18 November 2000). To detect a specific wave period, a sufficiently long time series is needed which covers several times this wave period [*Priestley*, 1989]. However, choosing a time period length that is much longer than the period in which the Kelvin waves are active will reduce the signal from the Kelvin waves. Taking into account these two counteracting factors, experimenting with different lengths of the time periods used in our calculations learned that 60 days is a suitable length for this study. The blue, green and red areas respectively denote the 90%, 99% and 99,9% significant signals. All three time periods show significant signals corresponding to eastward propagating waves 1–2 with periods of 15 days (1996, 1998) and 12 days (2000). These signatures agree with Kelvin wave characteristics.

[28] For comparison Figure 2a shows the periodogram P_N for time period P3 using total ozone columns from EP-TOMS averaged over 3 days on a $5° \times 5°$ mesh. The results are comparable to the results from the GOME GDP in Figure 1, only with a maximum at slightly longer wave periods of about 12–15 days.

[29] To check our significance criteria we have also calculated the periodogram using random data, see Figure 2b. As anticipated the periodogram does not exceed the 90% significance level at any wave number and period. When repeating the experiment numerous times, the periodogram hardly ever exceeds the 90% significance level and

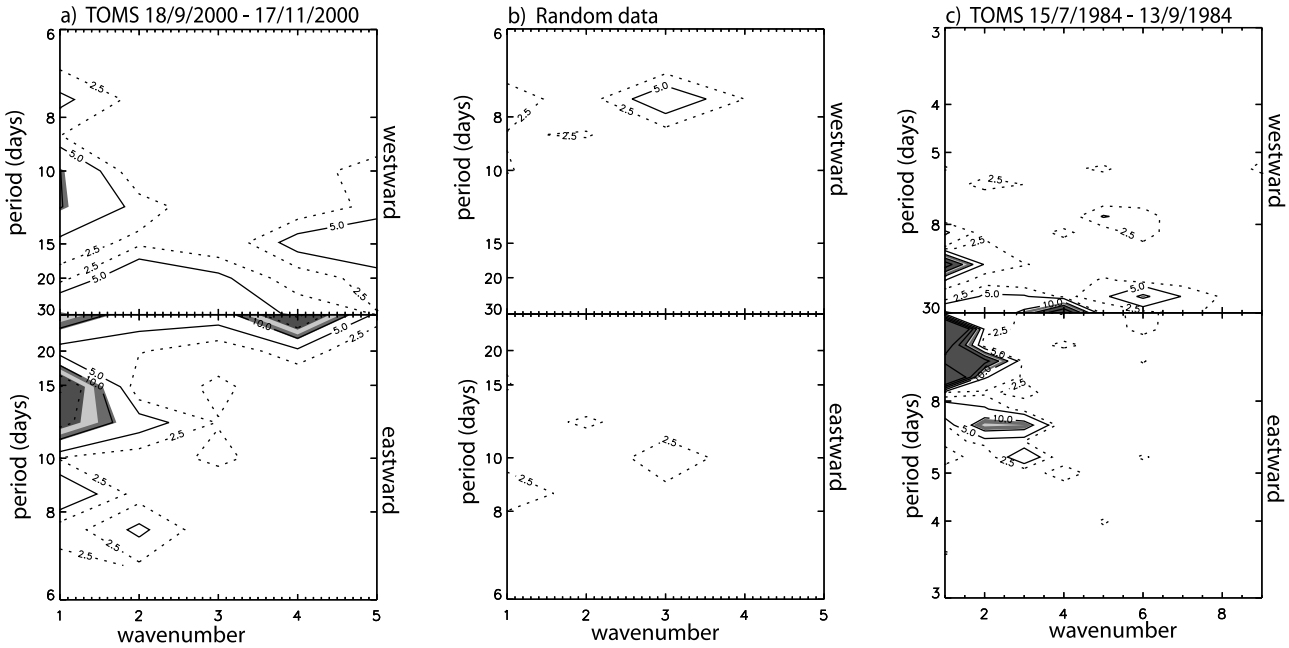

Figure 2. Lomb periodogram for (a) the 3-day averaged TOMS ozone columns in period P3, (b) random data, and (c) the 1-day averaged TOMS ozone columns in the period from 15 July to 13 September 1984. See color version of this figure at back of this issue.

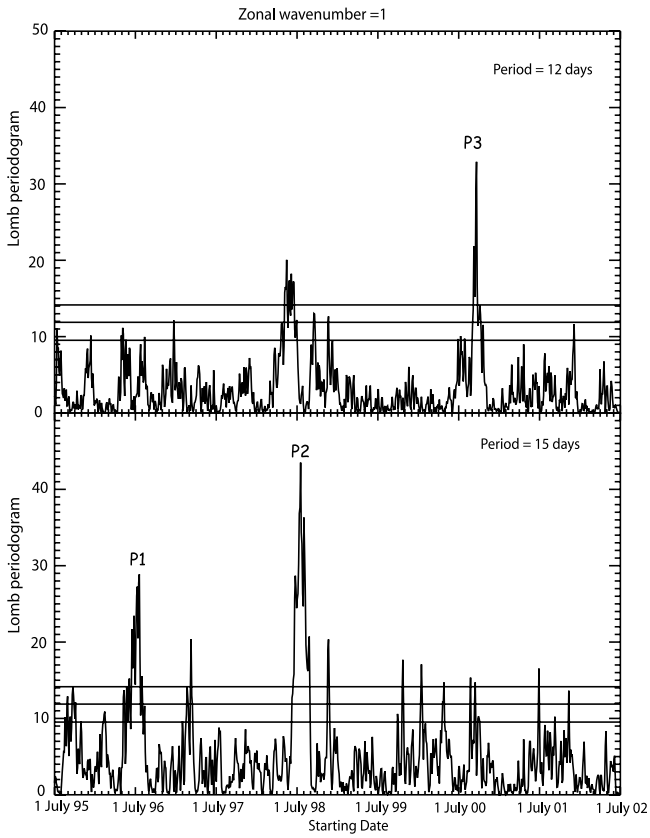

Figure 3. Time series of Lomb Periodogram for wave 1 at two specified frequencies. Upper plot corresponds to a wave period of 12 days and lower plot to a wave period of 15 days. The periodogram is plotted as function of the starting day of the 60-day time periods over which the periodogram is calculated.

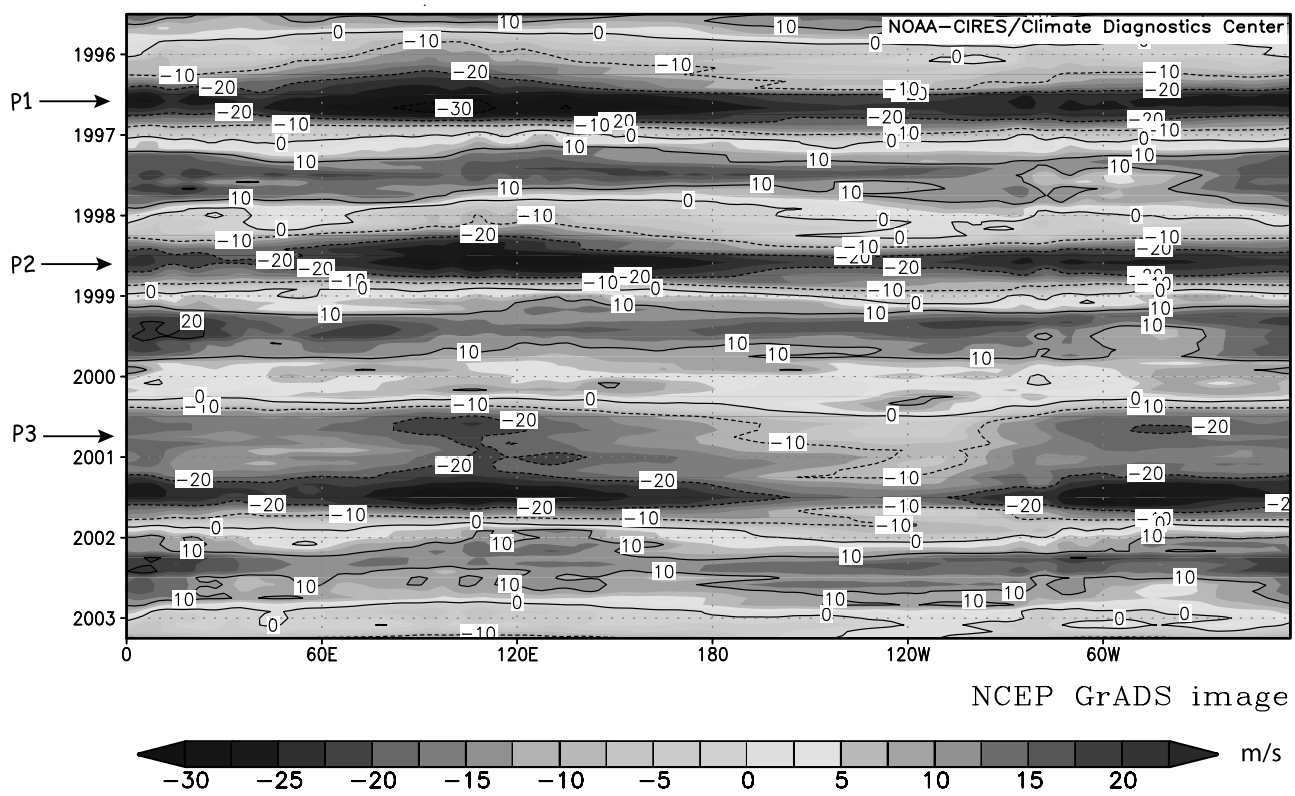

Figure 4. Monthly mean zonal wind [m/s] at 30 hPa at the equator for July 1995 to September 2002. (Image provided by the NOAA-CIRES Climate Diagnostics Center, Boulder, Colorado, USA, from their Web site at http://www.cdc.noaa.gov/.) See color version of this figure at back of this issue.

in none of the repetitions exceeds the 99% significance level (the probability for this is 1%).

[30] To compare our method with a more standard spectral approach we have also applied the Lomb periodogram to the Nimbus-7 TOMS total ozone column data analyzed in the work of *Ziemke and Stanford* [1994]. For this, the TOMS ozone columns are averaged over 1 day and regridded to a $5^\circ \times 5^\circ$ mesh. Figure 2 c shows the results for the period from 15 July to 13 September 1984. The plot shows a dominating signal from eastward waves 1 and 2 with periods between 8 and 30 days, which is in good agreement with the spectral amplitudes calculated by Ziemke and Stanford for the same period (see Figure 2a, period E2 in their paper).

[31] To find all episodes of high Kelvin wave activity in the 7-year time period from the start of the GOME operation in July 1995 until July 2002, we have plotted in Figure 3 the periodogram P_N, calculated over 60-day time periods, for wave 1 at two specific frequencies corresponding to wave periods of 12 and 15 days, as function of the starting date of the 60-day periods. The solid horizontal lines indicate the 90%, 99% and 99,9% significance levels. This figure clearly shows episodes of highest wave activity with wave periods of 15 days in 1996 and 1998, corresponding to the previously defined P1 and P2 periods, and an episode of highest wave activity with wave periods of 12 days in 2000, corresponding to period P3.

[32] NCEP reanalysis data [*Kalnay et al.*, 1996] of monthly mean zonal winds at 30 hPa for the same 7-year time period have been used to identify periods where strong Kelvin wave activity is expected. Figure 4 shows the zonal wind at 30 hPa at the equator. Periods P1, P2 and P3 are indicated with arrows. A clear correlation can be seen, especially in 1996 and 1998, between the wave activity and the westward zonal wind. This is in agreement with previous studies [*Shiotani and Horinouchi*, 1993], in which it was found that westward zonal wind at 30 hPa shows an in-phase relationship with lower stratospheric Kelvin wave activity.

[33] Figure 5 shows time versus longitude plots (commonly known as Hovmöller diagrams) for the three episodes P1, P2 and P3. The data are filtered as to retain only waves 1 and 2. Furthermore, in time a band-pass filter given by *Murakami* [1979] is applied with half amplitudes at 10 and 15 days. This filtering is applied to separate out the dominant frequencies shown in Figure 1. The Hovmöller diagrams give information on the propagation of waves with the selected frequencies, amplitudes of the ozone variations induced by these waves and can be used to determine the phase velocity of the waves. The plots reveal movements of the highest amplitudes that are eastward. The amplitudes are in the order of 1–2 DU, in agreement with model calculations by *Ziemke and Stanford* [1994]. The phase velocity of the waves, determined by taking the slope of lines through the amplitude maxima or minima, is between 25–45 m/s.

[34] Observed ozone perturbations are in the same order of magnitude as the noise in the 3-day averaged and gridded ozone columns (section 3). However this noise is distributed over all spatial and temporal frequencies in contrast to the

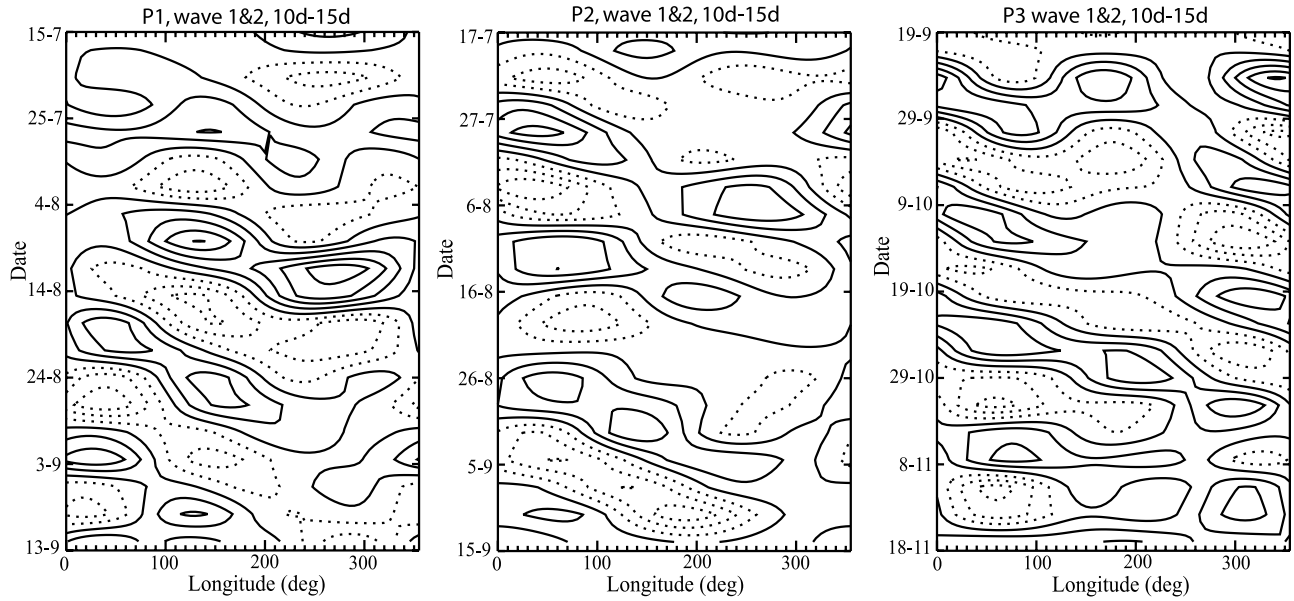

Figure 5. Hovmöller diagrams of waves 1 and 2 for time periods P1, P2 and P3. A band-pass filter with half-amplitudes at 10 and 15 days has been applied. Solid lines start at zero DU with an increment of 0.5 for each contour line. Dashed lines start at −0.5 DU with a decrement of 0.5 for each contour line.

Kelvin wave signatures which correspond to particular scales, i.e., specific frequencies and wave numbers [*Salby et al.*, 1990]. Only the fraction of the noise operating on those specific scales is relevant. If the error variance is distributed over all frequencies then the signal is an order of magnitude above the noise. Would this not be the case then it would be difficult to explain the signatures found at the specific frequencies and wave numbers corresponding to the dispersion characteristics of the equatorial Kelvin waves.

5. Outlook

[35] The spectral analysis method introduced in this paper can be applied to other satellite measurements.

[36] The total ozone record of GOME is extended by SCIAMACHY (Scanning Imaging Absorption Spectrometer for Atmospheric Chartography) [*Bovensmann et al.*, 1999], which is an extended version of GOME, launched on board ENVISAT in March 2002 and from 2005–2020 by the GOME-2 series on the METOP 1, 2 and 3 platforms.

[37] Combining the GOME total ozone record with the data from the SCIAMACHY and GOME-2 missions are anticipated to provide a 25-year time series of ozone column data (1995–2020) that allows the construction of a climatology of stratospheric Kelvin wave activity. A combination with the TOMS Nimbus-7 and Meteor-3 ozone column data sets (1978–1994) could be used to extend this time series. This however requires an homogenization of the two data sets.

[38] The features found in the GOME total ozone columns can be attributed to "slow" Kelvin waves in the lower stratosphere. However, profile measurements are needed to detect the vertical distribution of the Kelvin waves. Profile measurements also allow the same analysis, shown in this paper for total ozone columns, on separate stratospheric layers. Ozone profiles retrieved from the GOME nadir measurements [*van der A et al.*, 2002] will be analyzed to determine whether they can be used to detect Kelvin wave perturbations.

[39] In addition to nadir measurements, the SCIAMACHY instrument also performs limb measurements that will provide ozone profile data with a vertical resolution of ~3 km. The instrument observes the same air mass in limb and nadir viewing geometries within about 7 min. A combination of nadir column and limb profile measurements will offer the possibility for a better description of the 3-dimensional distribution of equatorial Kelvin wave activity.

6. Conclusion

[40] The extension of the unequally spaced data spectral technique first developed by Lomb from one to two dimensions makes it possible to analyze two dimensional data sets while profiting from the advantages of the Lomb periodogram. The main advantages are the applicability to unequally spaced data, like satellite data with gaps in space and time, and the possibility to evaluate the significance of observed spectral features.

[41] By applying this new method to seven years of GOME total ozone column measurements, we found spectral features which can be attributed to equatorial Kelvin waves in the lower stratosphere. These features are shown to be significant by exploiting the statistical behavior of the method.

[42] Three periods of high Kelvin wave activity have been identified in 1996, 1998 and 2000, which correlate to periods of westward equatorial zonal winds at 30 hPa. The three periods show eastward propagating waves 1–2 with periods of 12–15 days and induced ozone column variations around 2–4 DU peak-to-peak. The results agree with the characteristics of "slow" Kelvin waves in the lower stratosphere. The method has also been applied to TOMS ozone column data and shows results comparable to the results from using GOME data.

[43] This study makes a new contribution in the field of Kelvin wave analysis by introducing bidimensional unequally spaced data spectral analysis and demonstrates the sensitivity of the GOME ozone columns to tropical Kelvin waves, showing the potential of the GOME ozone measurements to contribute to a global description of equatorial Kelvin wave activity.

[44] **Acknowledgments.** The author would like to thank Folkert Boersma for the stimulating discussions and helpful comments and Pieter Valks for his valuable suggestions. GOME ozone products have been provided by DFD-DLR on behalf of ESA. NCEP Reanalysis data have been provided by the NOAA-CIRES Climate Diagnostics Center, Boulder, Colorado, USA, from their Web site at http://www.cdc.noaa.gov/.

References

Amodei, M., S. Pawson, A. A. Scaife, U. Langematz, W. Lahoz, D. M. Li, and P. Simon (2001), The SAO and Kelvin waves in the EuroGRIPS GCMS and the UK Meteorological Office analyses, *Ann. Geophys.*, *19*, 99–114.

Balis, D. S., C. Zerefos, A. Tsiropoulou, P. Taalas, and A. Anthis (2001), Validation of GOME total ozone using ground-based total ozone measurements from the WMO Global Atmosphere Watch, in *Proceedings of the SAF Training Workshop*, pp. 19–26, EUMETSAT, Halkidiki, Greece, 21–23 May.

Bovensmann, H., J. P. Burrows, M. Buchwitz, J. Frerick, S. Noël, V. V. Rozanov, K. V. Chance, and A. P. H. Goede (1999), SCIAMACHY: Mission objectives and measurement modes, *J. Atmos. Sci.*, *56*, 127–150.

Bramstedt, K., J. Gleason, D. Loyola, W. Thomas, A. Bracher, M. Weber, and J. P. Burrows (2002), Comparison of total ozone from the satellite instruments GOME and TOMS with measurements from the Dobson network 1996–2000, *Atmos. Chem. Phys. Discuss.*, *2*, 1131–1157.

Burrows, J. P., et al. (1998), The Global Ozone Monitoring Experiment (GOME): Mission concept and first scientific results, *J. Atmos. Sci.*, *56*, 151–175.

Canziani, P. O. (1999), Slow and ultraslow equatorial Kelvin waves: The UARS-CLAES view, *Q. J. R. Meteorol. Soc.*, *125*, 657–676.

Canziani, P. O., and J. R. Holton (1998), Kelvin waves and the quasi-biennial oscillation: An observational analysis, *J. Geophys. Res.*, *103*, 31,509–31,521.

Canziani, P. O., J. R. Holton, E. Fishbein, and L. Froidevaux (1995), Equatorial Kelvin wave variability during 1992 and 1993, *J. Geophys. Res.*, *100*, 5193–5202.

Canziani, P. O., J. R. Holton, E. Fishbein, L. Froidevaux, and J. W. Waters (1994), Equatorial Kelvin waves: A UARS-MLS view, *J. Atmos. Sci.*, *51*, 3053–3076.

Corlett, G. K., and P. S. Monks (2001), A comparison of total column ozone values derived from the Global Ozone Monitoring Experiment (GOME), the TIROS Operational Vertical Sounder (TOVS), and the Total Ozone Mapping Spectrometer (TOMS), *J. Atmos. Sci.*, *58*, 1103–1116.

Eskes, H. J., P. F. J. van Velthoven, P. J. M. Valks, and H. M. Kelder (2003), Assimilation of GOME total ozone satellite observations in a three-dimensional tracer transport model, *Q. J. R. Meteorol. Soc.*, *129*, 1663–1681.

Hamilton, K., R. J. Wilson, and R. S. Hemler (1999), Middle atmosphere simulated with high vertical and horizontal resolution versions of a GCM: Improvements in the cold pole bias and generation of a QBO-like oscillation in the tropics, *J. Atmos. Sci.*, *56*, 3829–3846.

Hirota, I. (1978), Equatorial waves in the upper stratosphere and mesosphere in relation to the semiannual oscillation of the zonal wind, *J. Atmos. Sci.*, *35*, 714–722.

Holton, J. R. (1992), *An Introduction to Dynamic Meteorology*, 3rd ed., Academic, San Diego, Calif.

Kalnay, E., et al. (1996), The NCEP/NCAR reanalysis 40-year project, *Bull. Am. Meteorol. Soc.*, *77*, 437–471.

Kawamoto, N., M. Shiotani, and J. C. Gille (1997), Equatorial Kelvin waves and corresponding tracer oscillations in the lower stratosphere as seen in LIMS data, *J. Meteorol. Soc. Jpn.*, *75*, 763–773.

Lambert, J.-C., et al. (2000), Combined characterisation of GOME and TOMS total ozone measurements from space using ground-based observations from the NDSC, *Adv. Space Res.*, *26*, 1931–1940.

Martin, R. V., et al. (2002), Interpretation of TOMS observations of tropical tropospheric ozone with a global model and in situ observations, *J. Geophys. Res.*, *107*(D18), 4351, doi:10.1029/2001JD001480.

Mc Peters, R. D., et al. (1998), Earth Probe Total Ozone Mapping Spectrometer (TOMS) data products user's guide, *NASA Tech. Publ. 1998-206895*.

Murakami, M. (1979), Large scale aspects of deep convective activity over the GATE area, *Mon. Weather Rev.*, *107*, 994–1013.

Pawson, S. (1992), A note concerning the inability of GCMs to model the QBO, *Ann. Geophys. Lett.*, *10*, 116–118.

Platt, U. (1994), Differential optical absorption spectroscopy (DOAS), in *Air Monitoring by Spectroscopic Techniques*, *Chem. Anal. Ser.*, vol. 127, edited by M. Siegrist, pp. 27–84, John Wiley, New York.

Press, W. H., S. A. Teukolsky, W. T. Vetterling, and B. P. Flannery (1992), *Numerical Recipes in Fortran (or in C or in Pascal): The Art of Scientific Computing*, 2nd ed., Cambridge Univ. Press, New York.

Priestley, M. B. (1989), *Spectral Analysis and Time Series*, Academic, San Diego, Calif.

Randel, W. J. (1990), Kelvin wave-induced trace constituent oscillations in the equatorial stratosphere, *J. Geophys. Res.*, *95*, 18,641–18,652.

Randel, W. J., and J. C. Gille (1991), Kelvin wave variability in the upper stratosphere observed in SBUV ozone data, *J. Atmos. Sci.*, *48*, 2336–2349.

Salby, M. L., D. L. Hartmann, P. L. Bailey, and J. C. Gille (1984), Evidence for equatorial Kelvin modes in Nimbus-7 LIMS, *J. Atmos. Sci.*, *41*, 220–235.

Salby, M. L., P. Callaghan, S. Solomon, and R. Garcia (1990), Chemical fluctuations associated with vertically propagating equatorial Kelvin waves, *J. Geophys. Res*, *95*, 20,491–20,505.

Scargle, J. D. (1982), Studies in astronomical time series analysis II. Statistical aspects of spectral analysis of unevenly spaced data, *Astrophys. J.*, *263*, 835–853.

Shiotani, M., and T. Horinouchi (1993), Kelvin wave activity and the quasi-biennial oscillation in the equatorial lower stratosphere, *J. Meteorol. Soc. Jpn.*, *71*, 175–181.

Shiotani, M., J. C. Gille, and A. E. Roche (1997), Kelvin waves in the equatorial lower stratosphere as revealed by cryogenic limb array etalon spectrometer temperature data, *J. Geophys. Res.*, *102*, 26,131–26,140.

Spurr, R., W. Thomas, and D. Loyola (2002), GOME level 1 to 2 algorithms description, *Tech. Note ER-TN-DLR-GO-0025, (Iss./Rev. 3/A)*, Dtsch. Zentrum fur Luft- und Raumfahrt, Inst. fur Method. der Fernerkundung, Köln, Germany, 31 July .

Stone, E. M., J. L. Stanford, J. R. Ziemke, D. R. Allen, F. W. Taylor, C. D. Rodgers, B. N. Lawrence, E. F. Fishbein, L. S. Elson, and J. W. Waters (1995), Space-time integrity of improved stratospheric and mesospheric sounder and microwave limb sounder temperature fields at Kelvin wave scales, *J. Geophys. Res.*, *100*, 14,089–14,096.

Takahashi, M. (1996), Simulation of the stratospheric quasi-biennial oscillation using a general circulation model, *Geophys. Res. Lett.*, *23*, 661–664.

Takahashi, M. (1999), Simulation of the quasi-biennial oscillation in a general circulation model, *Geophys. Res. Lett.*, *26*, 1307–1310.

Valks, P. J. M., R. B. A. Koelemeijer, M. van Weele, P. van Velthoven, J. P. F. Fortuin, and H. Kelder (2003), Variability in tropical tropospheric ozone: Analysis with Global Ozone Monitoring Experiment observations and a global model, *J. Geophys. Res.*, *108*(D11), 4328, doi:10.1029/2002JD002894.

van der A, R. J., R. F. van Oss, A. J. M. Piters, J. P. F. Fortuin, Y. J. Meijer, and H. M. Kelder (2002), Ozone profile retrieval from recalibrated Global Ozone Monitoring Experiment data, *J. Geophys. Res.*, *107*(D15), 4239, doi:10.1029/2001JD000696.

Wallace, J. M., and V. E. Kousky (1968), Observational evidence of Kelvin waves in the tropical stratosphere, *J. Atmos. Sci.*, *25*, 900–907.

Ziemke, J. R., and J. L. Stanford (1994), Kelvin waves in total column ozone, *Geophys. Res. Lett.*, *21*, 105–108.

H. M. Kelder, R. M. A. Timmermans, and R. F. van Oss, Royal Netherlands Meteorological Institute, P.O. Box 201, 3730 AE De Bilt, Netherlands. (kelder@knmi.nl; renske.timmermans@knmi.nl; ossvanr@knmi.nl)

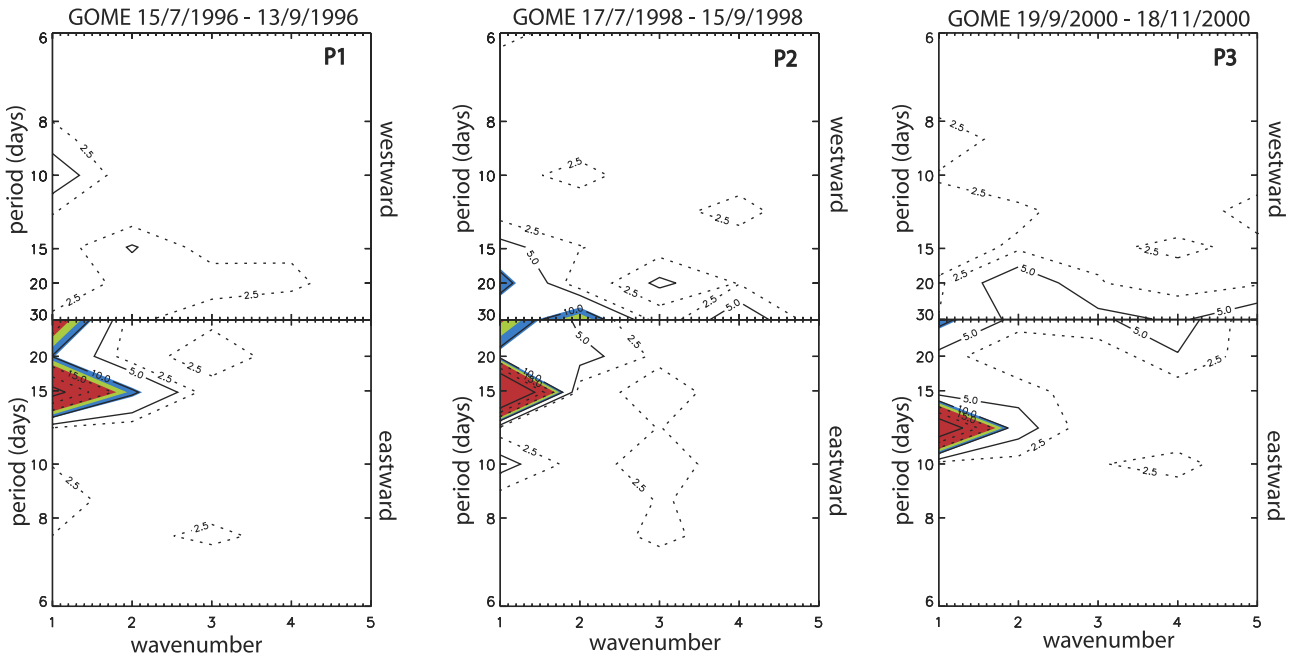

Figure 1. Lomb periodogram for the GOME ozone columns for three different periods.

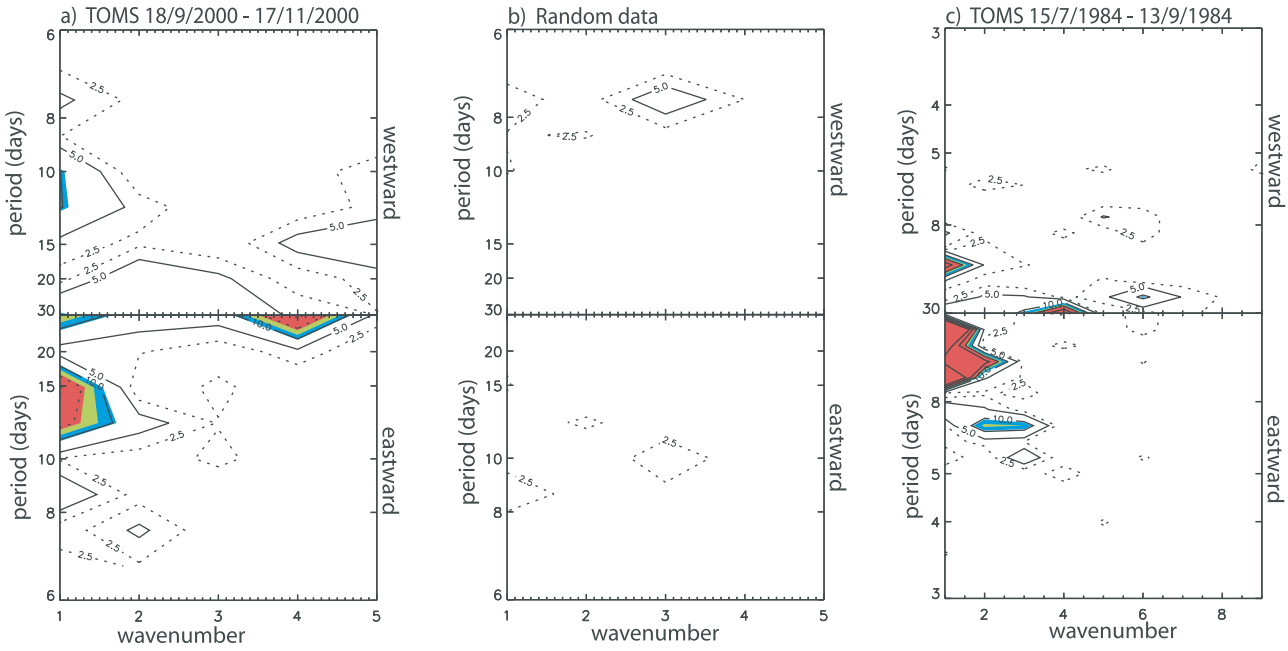

Figure 2. Lomb periodogram for (a) the 3-day averaged TOMS ozone columns in period P3, (b) random data, and (c) the 1-day averaged TOMS ozone columns in the period from 15 July to 13 September 1984.

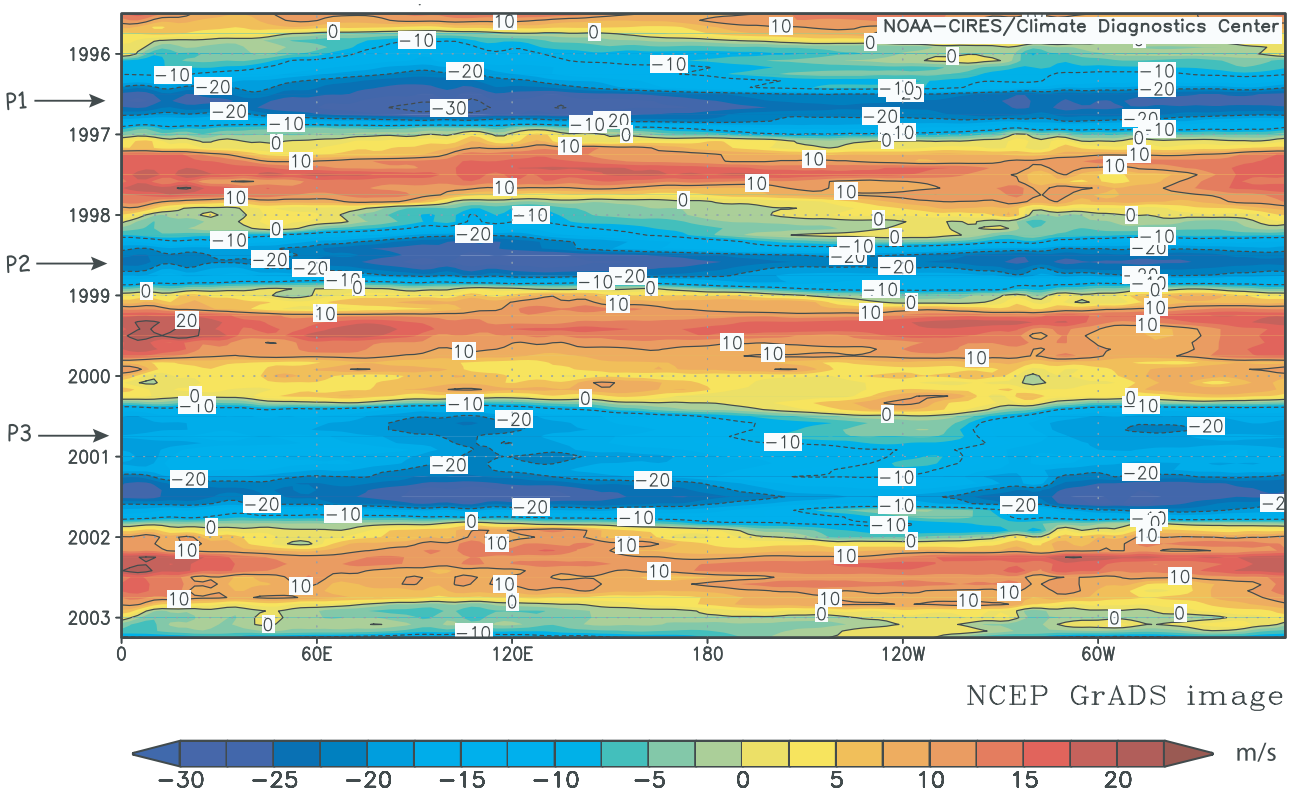

Figure 4. Monthly mean zonal wind [m/s] at 30 hPa at the equator for July 1995 to September 2002. (Image provided by the NOAA-CIRES Climate Diagnostics Center, Boulder, Colorado, USA, from their Web site at http://www.cdc.noaa.gov/.)